JCB Article

The Abl-related gene (Arg) requires its F-actin–microtubule cross-linking activity to regulate lamellipodial dynamics during fibroblast adhesion

Ann L. Miller,[1] Yinxiang Wang,[1] Mark S. Mooseker,[2,3,4] and Anthony J. Koleske[1,5]

[1]Department of Molecular Biophysics and Biochemistry, [2]Department of Molecular, Cellular, and Developmental Biology, [3]Department of Cell Biology, [4]Department of Pathology, and [5]Interdepartmental Neuroscience Program, Yale University, New Haven, CT 06520

Microtubules (MTs) help establish and maintain cell polarity by promoting actin-dependent membrane protrusion at the leading edge of the cell, but the molecular mechanisms that mediate cross-talk between actin and MTs during this process are unclear. We demonstrate that the Abl-related gene (Arg) nonreceptor tyrosine kinase is required for dynamic lamellipodial protrusions after adhesion to fibronectin. *arg*$^{-/-}$ fibroblasts exhibit reduced lamellipodial dynamics as compared with wild-type fibroblasts, and this defect can be rescued by reexpression of an Arg-yellow fluorescent protein fusion. We show that Arg can bind MTs with high affinity and cross-link filamentous actin (F-actin) bundles and MTs in vitro. MTs concentrate and insert into Arg-induced F-actin–rich cell protrusions. Arg requires both its F-actin–binding domains and its MT-binding domain to rescue the defects in lamellipodial dynamics of *arg*$^{-/-}$ fibroblasts. These findings demonstrate that Arg can mediate physical contact between F-actin and MTs at the cell periphery and that this cross-linking activity is required for Arg to regulate lamellipodial dynamics in fibroblasts.

Introduction

The development of a multilayered organism and the maintenance and repair of its tissues require cell migrations that must be performed with exquisite spatial and temporal precision. The actin cytoskeleton provides the force for cell migration. Actin polymerization drives protrusion of the cell's leading edge, whereas retrograde actin flow in the cell body provides traction for cell body movement (Mitchison and Cramer, 1996; Suter and Forscher, 1998; Pollard and Borisy, 2003). The localization and activation of actin-based force-generating complexes must be carefully controlled to generate directed cell movement.

Dynamic interplay between the actin and microtubule (MT) cytoskeletons is required for the coordination of actin-based cell movement (Bershadsky et al., 1991; Vasiliev, 1991). As cells migrate, they extend lamellipodia at their leading edge. In many polarized motile cells, MTs align along the axis of migration with their plus ends extended in the direction of cell movement (Vasiliev, 1991), and MT extension into the cell periphery is required for lamellipodial protrusion at the leading edge (Waterman-Storer et al., 1999). In early discussions of the dynamic properties of MTs, Kirschner and Mitchison (1986) proposed that MT plus ends might assume a polarized distribution by targeting and interacting stably with specific sites in the cell periphery. Subsequent studies have shown that MT plus ends are captured at the cell periphery by the interaction of MT plus end–binding proteins (Gundersen, 2002; Rodriguez et al., 2003). MT capture sites in the cortical actin network are defined through the localized activation of the Rho family GTPase Cdc42 and protein kinases by cell surface receptors (Etienne-Manneville and Hall, 2001, 2003a,b). However, the protein components of these MT capture sites and the molecular mechanisms that regulate their formation and stability remain unclear.

Abl family kinases, which include the mammalian Abl and Abl-related gene (Arg) proteins, regulate cell migration and

Y. Wang made significant contributions to this paper.

The online version of this article contains supplemental material.

Address correspondence to Anthony J. Koleske, Department of Molecular Biophysics and Biochemistry, Yale University, SHMC-E31, 333 Cedar St., New Haven, CT 06520. Tel.: (203) 785-5624. Fax: (203) 785-7979. email: anthony.koleske@yale.edu

Key words: cytoskeleton; actin; microtubules; protein-tyrosine kinase; Arg tyrosine kinase

Abbreviations used in this paper: Arg, Abl-related gene; MT, microtubule.

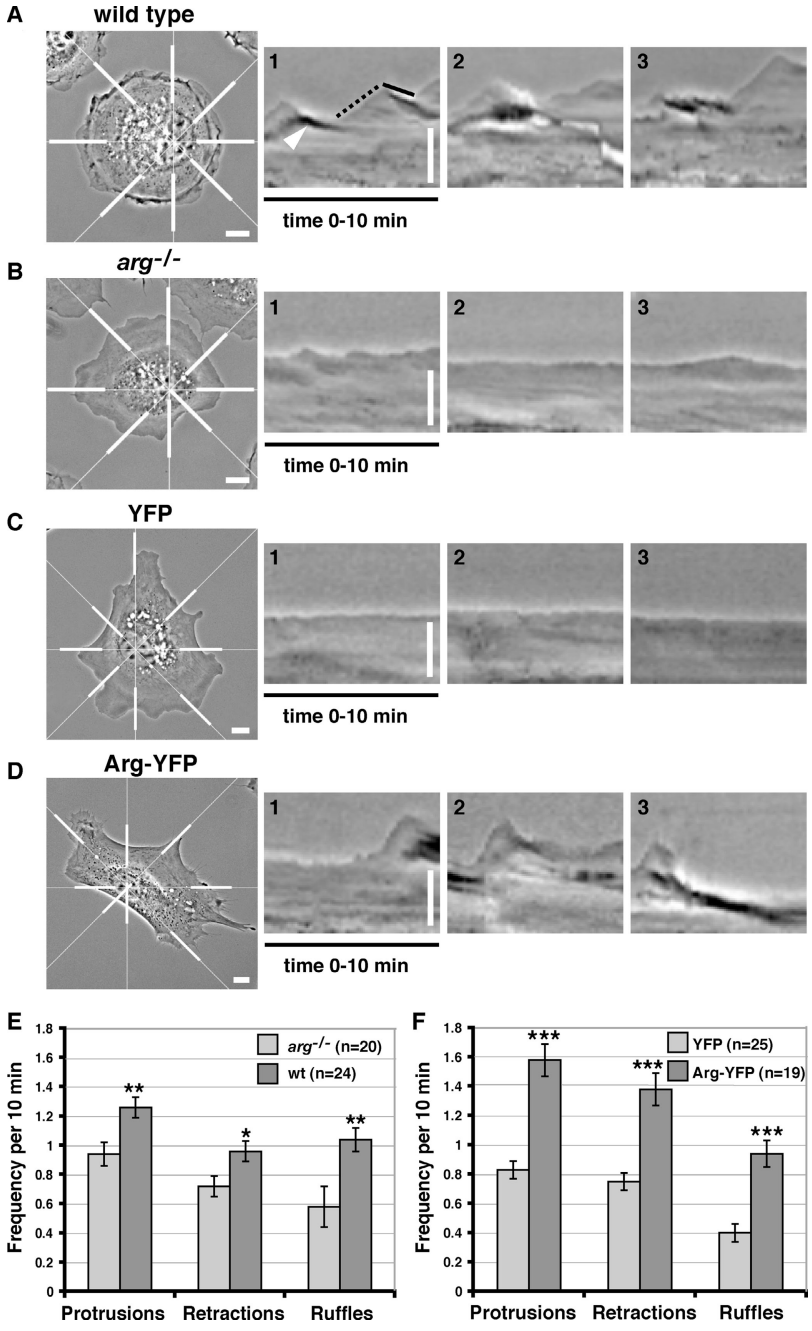

Figure 1. **Arg promotes lamellipodial dynamics in adhering fibroblasts.** (A–D) The leftmost panels are individual frames from time-lapse movies of (A) wild-type, (B) $arg^{-/-}$, (C) $arg^{-/-}$ + YFP, (D) or $arg^{-/-}$ + Arg-YFP cells. For kymographic analysis, a radial grid of eight lines was centered on the nucleus of the phase-contrast images (as shown in the left panels of A–D). Kymographs illustrating the lamellipodial activity during the 10-min time-lapse movies were made at eight places around the edge of the cells (indicated by thick white bars). Examples of the kymographs generated for the cells in A–D are shown in the right three panels for each. Ascending edges (A, dotted black line) and descending edges (A, solid black line) indicate protrusion and retraction events. An example of a phase-dense membrane ruffle is indicated by the white arrowhead in A. Time is in the horizontal direction, and distance is in the vertical direction. Bars, 10 μm. (E) Frequencies of protrusions, retractions, and phase-dense membrane ruffles were quantified and averaged for $arg^{-/-}$ ($n = 20$) and wild-type cells ($n = 24$) at eight places around the cell periphery for each cell. The differences in frequencies of protrusion, retraction, and phase-dense ruffling between the wild-type and $arg^{-/-}$ cells were statistically significant by *t* test (**, $P < 0.006$; *, $P < 0.05$). (F) The same criteria were measured for YFP-expressing $arg^{-/-}$ cells ($n = 25$) and Arg-YFP–expressing $arg^{-/-}$ cells ($n = 19$) at eight places around the cell periphery for each cell. The differences in frequencies of protrusion, retraction, and phase-dense ruffling between the $arg^{-/-}$ + YFP and $arg^{-/-}$ + Arg-YFP cells were statistically significant by *t* test (***, $P < 0.00001$). Error bars represent mean ± SEM.

morphogenesis in developing metazoa (Gertler et al., 1989; Giniger, 1998; Koleske et al., 1998; Wills et al., 1999a,b; Bashaw et al., 2000; Zukerberg et al., 2000; Grevengoed et al., 2001). Abl family kinases help translate signals from cell surface receptors into changes in cytoskeletal structure (Moresco and Koleske, 2003; Hernández et al., 2004a). Activation of growth factor or adhesion receptors leads to increased Abl kinase activity (Plattner et al., 1999; Renshaw et al., 2000; Frasca et al., 2001; Howe et al., 2002), and this increased kinase activity promotes cytoskeletal rearrangements leading to increased membrane ruffling (Plattner et al., 1999) and reduced cell migration (Frasca et al., 2001; Kain and Klemke, 2001).

Abl family kinases regulate cell motility and morphology by targeting several different cellular substrates. The finding that Abl phosphorylates the focal adhesion proteins Crk (Kain and Klemke, 2001) and paxillin (Salgia et al., 1995; Lewis and Schwartz, 1998) suggests that Abl may influence cell adhesion and motility by controlling the stability of focal adhesions. Abl family kinases can also regulate cytoskeletal dynamics by controlling the activity of Rho family GTPases. The 190-kD GTPase-activating protein for Rho (p190RhoGAP) is a major substrate of Arg in the developing postnatal mouse brain. Arg phosphorylation of p190RhoGAP activates its RhoGAP activity and promotes neurite outgrowth from neuroblastoma cells (Hernández et al., 2004b).

Arg's COOH-terminal half contains two distinct F-actin–binding domains, which it can use to organize the cytoskeleton directly. Arg binds cooperatively to F-actin during bundle formation, and binding saturates at a ratio of 1 Arg/2 actin

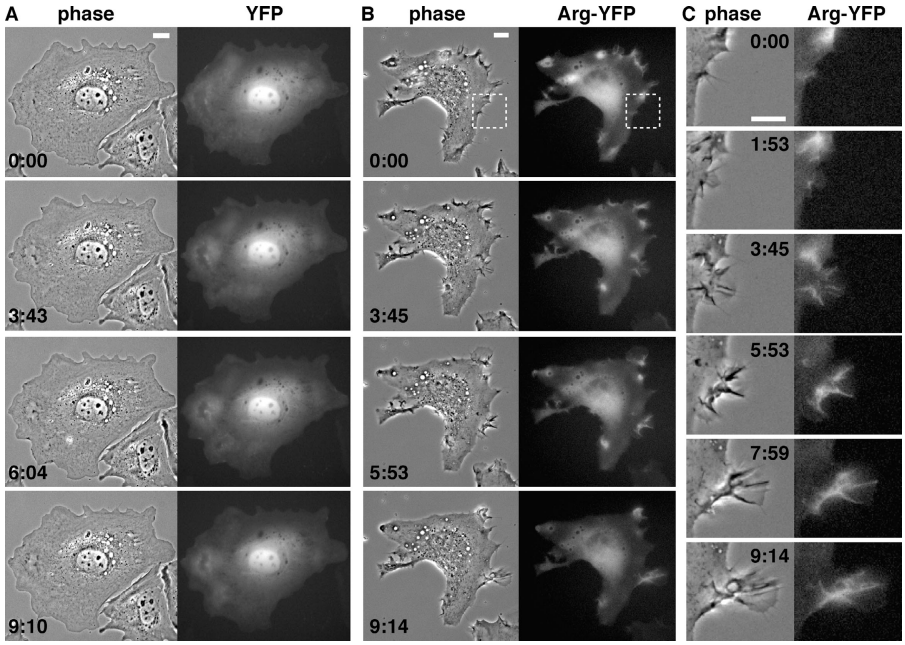

Figure 2. **Arg-YFP is concentrated at sites of lamellipodial protrusion and phase-dense membrane ruffling.** (A and B) Individual frames from time-lapse movies of *arg*$^{-/-}$ cells expressing YFP (A; Video 1) or Arg-YFP (B; Video 2). Phase-contrast images are on the left, and fluorescence images are on the right. (C) Enlargement of the region boxed in the top row of B showing a protrusive structure induced in the Arg-YFP–expressing cell (Video 3). Elapsed time, min:s. Bars, 10 μm.

monomers (Wang et al., 2001). An Arg-YFP fusion concentrates at discrete sites in the cell periphery where it induces localized F-actin concentrations (Wang et al., 2001). An Arg COOH-terminal fragment containing Arg's two F-actin–binding domains is necessary and sufficient to bundle F-actin in vitro and can induce F-actin–rich structures in cells (Wang et al., 2001). These experiments argue that Arg can use its F-actin–bundling activity to organize actin structures in vivo in a manner that is independent of kinase activity.

We show here that upon adhesion to fibronectin, *arg*$^{-/-}$ fibroblasts exhibit fewer episodes of lamellipodial protrusion, lamellipodial retraction, and phase-dense membrane ruffling as compared with wild-type fibroblasts. Expression of Arg-YFP in *arg*$^{-/-}$ fibroblasts rescues these defects. We report that Arg has a MT-binding domain located between its two F-actin–binding domains and that Arg can cross-link F-actin and MTs in vitro. Arg-YFP localizes with F-actin at sites of lamellipodial protrusion and membrane ruffling, and MTs insert into these Arg-induced F-actin–rich membrane protrusions. An Arg COOH-terminal fragment containing both F-actin–binding domains and the MT-binding domain can rescue the lamellipodial defects of *arg*$^{-/-}$ fibroblasts, but an Arg mutant lacking part of the MT-binding domain fails to rescue these defects. Our studies show that Arg requires its F-actin–MT cross-linking activity to regulate lamellipodial dynamics in fibroblasts. We propose that localized concentrations of Arg may help organize MT-capture sites at the cell periphery, leading to increased targeting of MTs and increased lamellipodial dynamics.

Results

Arg promotes lamellipodial dynamics in adhering fibroblasts

Wild-type fibroblasts plated on fibronectin exhibit an irregular, dynamic cell periphery as the cells sample, adhere, and spread on their new adhesive substrate. In contrast to this behavior, *arg*$^{-/-}$ fibroblasts exhibit a smooth, nearly static lamellar appearance upon adhesion to fibronectin. 10-min time-lapse movies of wild-type and *arg*$^{-/-}$ fibroblasts were analyzed by kymography to quantify the frequency and rate of lamellipodial protrusion, lamellipodial retraction, and phase-dense membrane ruffling (Hinz et al., 1999). Wild-type cells exhibited cycles of lamellipodial protrusion and retraction and phase-dark membrane ruffles, yielding kymographs that looked like "rolling hills" (Fig. 1, A and E). In contrast, Arg-deficient fibroblasts exhibited significantly less frequent episodes of lamellipodial protrusion, lamellipodial retraction, and phase-dense membrane ruffling than wild-type fibroblasts, yielding more featureless "prairie-like" kymographs (Fig. 1, B and E). Although they appear less frequently in the *arg*$^{-/-}$ cells, the mean rate and distance of lamellipodial protrusions and retractions were similar to those in wild-type cells (unpublished data).

Our previous studies showed that an Arg-YFP fusion promotes the formation of F-actin–rich structures at the fibroblast periphery (Wang et al., 2001). We examined whether reexpression of Arg-YFP in *arg*$^{-/-}$ fibroblasts could correct the deficiencies in lamellipodial dynamics and membrane ruffling of *arg*$^{-/-}$ cells. *arg*$^{-/-}$ fibroblasts were infected with retroviruses expressing YFP or Arg-YFP, and YFP-positive cells were selected by fluorescence-activated cell sorting. The periphery of the YFP-expressing *arg*$^{-/-}$ fibroblasts spreading on fibronectin was composed of mostly smooth lamellae that did not change significantly during a 10-min filming period (Fig. 2 A; Video 1, available at http://www.jcb.org/cgi/content/full/jcb.200308055/DC1). The YFP signal was distributed diffusely throughout the nucleus and cytoplasm (Fig. 2 A; Video 1). Kymographs of YFP-expressing cells had the "prairie-like" appearance of control *arg*$^{-/-}$ fibroblasts (Fig. 1, C and F). Not surprisingly, the frequencies of lamellipodial protrusions, lamellipodial retractions, and phase-dense membrane ruffles were similar for both YFP-expressing *arg*$^{-/-}$ cells (Fig. 1 F) and uninfected *arg*$^{-/-}$ cells (Fig. 1 E).

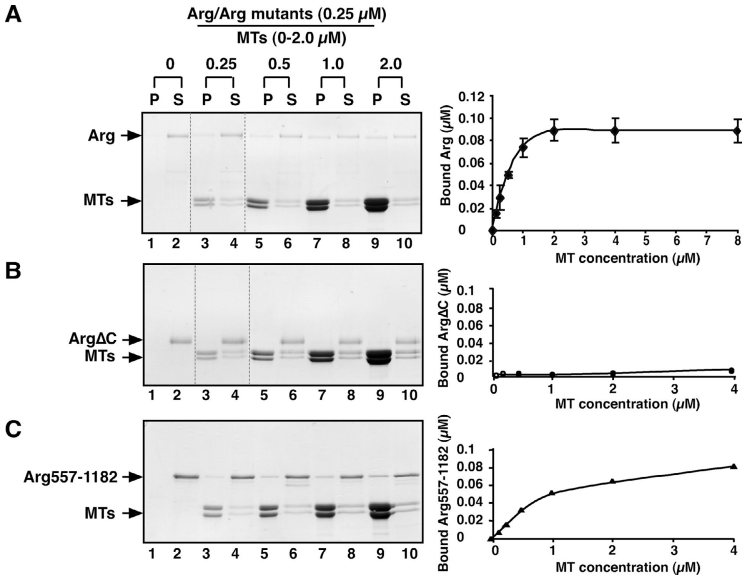

Figure 3. **Arg binds MTs.** (A–C) Cosedimentation of Arg or Arg mutants with MTs. (A) A fixed concentration of 0.25 μM Arg was mixed with increasing concentrations of MTs from 0 to 2 μM. The mixture was then pelleted by centrifugation, and equivalent amounts of the pellet (P) and supernatant (S) fractions were separated by SDS-PAGE followed by Coomassie blue staining. The amount of Arg or Arg mutants bound to MTs was quantified by densitometry. Three independent binding assays were repeated with 0.25 μM Arg and 0–8 μM MTs, and a plot of MT concentration (x axis) versus the amount Arg bound (y axis) is shown on the right. The dashed lines in A and B indicate places where two gels were spliced together. Lanes 1–4 are from one gel, and lanes 5–10 are from another gel. (B and C) 0.25 μM ArgΔC (B) or Arg557-1182 (C) was mixed with increasing concentrations of MTs from 0 to 2 μM and treated as described in A. A plot of MT concentration (x axis) versus the amount Arg mutant bound (y axis) is shown on the right.

Expression of Arg-YFP complemented the deficiencies in lamellipodial dynamics and membrane ruffling of *arg*$^{-/-}$ cells. The periphery of Arg-YFP–expressing *arg*$^{-/-}$ fibroblasts was highly irregular and dynamic, containing multiple protrusions and phase-dense ruffles (Fig. 2, B and C; Videos 2 and 3, available at http://www.jcb.org/cgi/content/full/jcb.200308055/DC1). Consistent with a role in the regulation of lamellipodial dynamics, the Arg-YFP signal was concentrated in areas of lamellipodial protrusion and phase-dense ruffling (Fig. 2, B and C; Videos 2 and 3). To confirm that the concentration of Arg-YFP at the periphery was due to its interaction with F-actin and not simply due to increased cell volume, we simultaneously monitored YFP or Arg-YFP localization, F-actin, and cell volume (with CellTracker® orange reagent; Fig. S1, available at http://www.jcb.org/cgi/content/full/jcb.200308055/DC1). Kymographs of the Arg-YFP–expressing *arg*$^{-/-}$ cells exhibited the "rolling hill" profile (Fig. 1, D and F), similar to that of wild-type cells. In fact, the frequencies of lamellipodial protrusions and retractions were actually higher in the Arg-YFP–expressing *arg*$^{-/-}$ cells (Fig. 1 F) than in wild-type cells (Fig. 1 E). Immunoblotting of lysates from wild-type cells and *arg*$^{-/-}$ cells expressing Arg-YFP (using dilutions of purified recombinant Arg as standards) revealed that Arg-YFP was expressed at 2.3-fold over wild-type Arg levels (unpublished data). The elevated frequency of lamellipodial dynamics in Arg-YFP–expressing cells over wild-type levels may result from this modest level of overexpression.

Arg binds MTs

MT extension into the cell periphery is required for the formation of actin-dependent membrane protrusions (Waterman-Storer et al., 1999). Our finding that Arg-YFP promotes membrane protrusion suggested that Arg might interact with MTs in this process. For example, Arg might promote membrane protrusion by tethering MTs to localized regions of the cell periphery. We used a cosedimentation assay to test whether purified recombinant Arg could bind MTs (Fig. 3 A). Arg was mixed with increasing concentrations of taxol-stabilized MTs assembled from MAP-free tubulin. After high speed centrifugation at 120,000 *g*, we measured the amount of Arg cosedimenting with MTs in the pellet fraction. When incubated alone, Arg remained in the supernatant after centrifugation (Fig. 3 A, lanes 1 and 2). However, when incubated with MTs, a portion of Arg was recovered in the pellet fraction, demonstrating an association of Arg with MTs (Fig. 3 A, lanes 3, 5, 7, and 9). The amount of Arg bound to MTs increased with MT concentration. Arg bound MTs with a K_d = 0.44 μM (Fig. 3 A). We determined a similar binding constant (K_d = 0.43 μM) by monitoring Arg binding to 1 μM MTs as a function of Arg concentration (Fig. S2, available at http://www.jcb.org/cgi/content/full/jcb.200308055/DC1). This analysis also revealed that Arg binding to MTs saturates at a ratio of 0.82 Arg molecules/1 tubulin dimer (Fig. S2). Unlike the binding of Arg to F-actin, Arg does not cross-link MTs as assessed by both light microscopy and electron microscopy of negatively stained preparations of MT–Arg mixtures (unpublished data).

MT binding to Arg deletion mutants (Table I) was assessed to identify the region of Arg that interacts with MTs. An Arg mutant lacking all amino acids COOH-terminal to the kinase domain (ArgΔC) failed to bind MTs (Fig. 3 B). However, an Arg COOH-terminal fragment (Arg557-1182) bound MTs with a slightly reduced affinity (K_d = 1.55 μM; Fig. 3 C) as compared with full-length Arg. These experiments indicated that the MT-binding domain is located in Arg's COOH-terminal half.

An Arg mutant lacking amino acids 930–1140 (ArgΔ930-1140) failed to bind MTs (Fig. 4 A) but did bind F-actin (not depicted), suggesting that the internal F-actin–binding domain (residues 688–930) was still folded properly. An Arg557-1140 fragment still bound MTs, albeit with a reduced affinity (K_d = 6.5 μM; Fig. 4 B) as compared with full-length Arg or the Arg COOH-terminal domain. A GST fusion to Arg residues 557–930 failed to bind MTs (unpublished data). Together, these data suggest that residues within amino acids 930–1140 are required for detectable Arg binding to MTs.

Table I. **Summary of microtubule binding and cross-linking of microtubules and F-actin by Arg or Arg mutants**

		MT binding	Cross-linking of MTs and F-actin
Arg	SH3 SH2 Kinase F MT F	+	+
ArgΔC	SH3 SH2 Kinase	−	−
Arg557-1182	F MT F	+	+
Arg557-1140	F MT	+	+
ArgΔ930-1140	SH3 SH2 Kinase F	−	−
ArgΔ858-1034	SH3 SH2 Kinase F F	−	−
GST-557-930	GST F	−	−
GST-930-1140	GST MT	+	NT
GST-924-1090	GST MT	+	NT
GST-930-1060	GST MT	−	NT
GST-930-980	GST	−	NT
GST-980-1060	GST	−	NT
GST-984-1054	GST	−	NT
GST-1034-1182	GST F	−	NT

NT, not tested.

The potential MT binding activity associated with residues 930–1140 was examined using GST fusion proteins containing this region of Arg. GST-924-1090 could bind to MTs (Fig. 4 C). Because GST-924-1090 and MTs comigrate on SDS-PAGE gels, immunoblot analysis with anti-GST antibodies was performed to determine the amount of GST-924-1090 in the supernatant and pellet fractions (Fig. 4 C). No binding of GST alone to MTs was detected (Fig. 4 D). However, GST-924-1090 binding to MTs did not reach saturation, thus preventing us from estimating the affinity of this fragment for MTs accurately (although a lower limit of $K_d > 1.3$ μM can be placed on this interaction). Although GST-924-1090 bound MTs, smaller fragments of the MT-binding domain (930-980, 930-1060, 980-1060) failed to bind MTs. The MT-binding properties of Arg deletion mutants and fragments are summarized in Table I. Sequence alignments of the minimal MT binding domain of Arg (amino acids 924–1090) with known MT binding proteins revealed a proline-rich stretch of amino acids in Arg that is 37% identical (43% similar) to a proline-rich stretch of amino acids near the COOH terminus of the GTPase dynamin that has been reported to bind MTs (Herskovits et al., 1993; Fig. S3, available at http://www.jcb.org/cgi/content/full/jcb.200308055/DC1).

Arg cross-links MTs and F-actin in vitro

The demonstration that Arg binds to both MTs and F-actin suggests that it could indeed play a critical role in coordinating the interaction of MTs and F-actin at the cell periphery. However, it was important to assess whether MT-associated

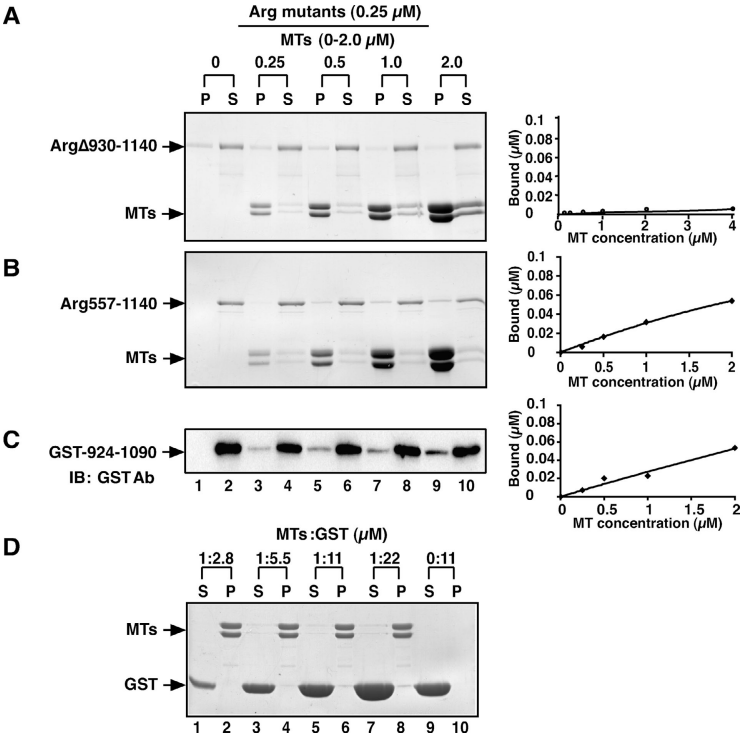

Figure 4. **Localization of the Arg MT-binding domain.** (A and B) Cosedimentation of ArgΔ930-1140 (A) or Arg557-1140 (B) with MTs as described for Fig. 3 A. (C) Cosedimentation of GST-924-1090 with MTs. Because of the similar mobility of GST-924-1090 and MTs by SDS-PAGE, immunoblot analysis with anti-GST antibodies was performed to detect binding of GST-924-1090 to MTs. The amount of the Arg mutants bound to MTs in A–C was quantified by densitometry, and the resulting plots of MT concentration (x axis) versus the amount Arg mutant bound (y axis) are shown to the right of the cosedimentation gels. (D) Control demonstrating that GST alone does not bind to MTs.

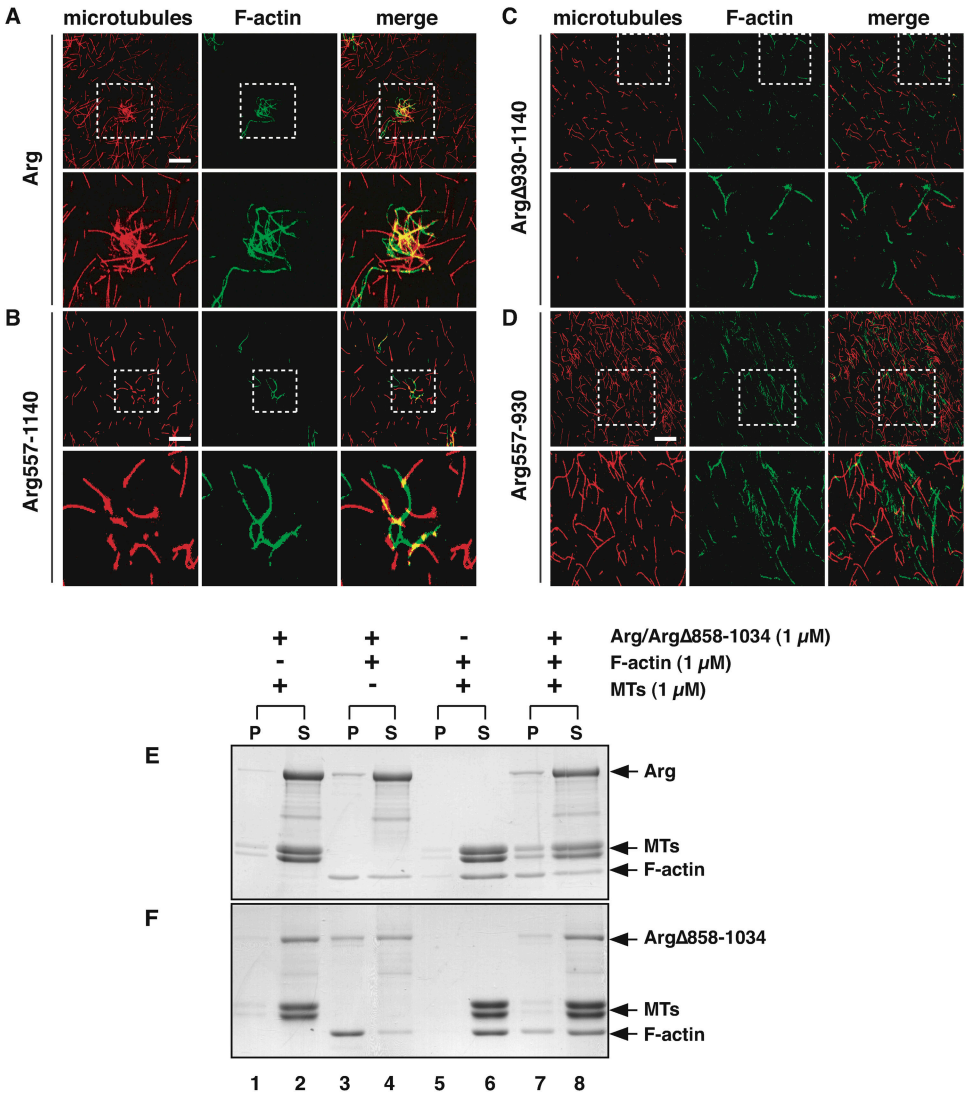

Figure 5. **Arg cross-links MTs and F-actin in vitro.** (A–D) Purified Arg or Arg mutant proteins (0.5 μM) were mixed with rhodamine-labeled MTs (red; 1 μM). Alexa 488-phalloidin–labeled F-actin (green; 1 μM) was added to the mixture, samples were plated on glass coverslips, and were visualized by fluorescence microscopy. (A) Arg; (B) Arg557-1140; (C) ArgΔ930-1140; (D) Arg557-930. Enlargements of the boxed regions are shown in the panels directly below. Bars, 20 μm. (E and F) Cross-linking of Arg (E) or ArgΔ858-1034 (F), F-actin, and MTs by low speed sedimentation. 1 μM Arg (E) or ArgΔ858-1034 (F) was incubated with 1 μM MTs and 1 μM F-actin (lanes 7 and 8), and the mixture was pelleted by centrifugation at 5,000 *g* for 10 min to pellet F-actin bundles and F-actin cross-linked MTs. The pellet (P) and supernatant (S) fractions were separated by SDS-PAGE followed by Coomassie blue staining. As a control, (E) Arg or (F) ArgΔ858-1034 was mixed with MTs (lanes 1 and 2) or F-actin (lanes 3 and 4) and subjected to centrifugation, and MTs and F-actin (lanes 5 and 6) were mixed and subjected to centrifugation.

Arg retains the ability to bind F-actin, because both the MT- and actin–binding activities lie within the COOH-terminal half of Arg. Alexa 488-phalloidin–labeled F-actin was added to rhodamine-labeled MTs that had been preincubated with Arg. This resulted in the formation of cross-linked arrays of MTs and F-actin, which could be visualized by fluorescence microscopy (Rothenberg et al., 2003; Fig. 5 A). We demonstrated previously that Arg is a monomer in solution (Wang et al., 2001), suggesting that these cross-linked structures did not result from nonspecific aggregation of Arg. These observations indicate that Arg can simultaneously bind both MTs and actin filaments. The finding that ArgΔ930-1140 failed to cross-link MTs and F-actin (Fig. 5 C), suggested that the MT-binding domain was essential for the MT/F-actin cross-linking activity. An Arg fragment containing just the internal F-actin–binding domain and the MT-binding domain (Arg557-1140) cross-linked MTs and F-actin in this assay (Fig. 5 B), although the structures formed were fewer and smaller than those formed with full-length Arg. An Arg fragment containing the internal F-actin–binding domain alone (Arg557-930) failed to cross-link MTs and F-actin (Fig. 5 D). A summary of the F-actin–MT cross-linking activity of Arg and several Arg mutants is presented in Table I.

The ability of Arg to cross-link MTs and actin was also assessed by low speed sedimentation. When incubated separately, Arg, MTs, and F-actin each remained in the supernatant after low speed centrifugation at 5,000 *g* (unpublished data). Under these conditions, Arg did not affect the sedimentation of MTs when both proteins were mixed (Fig. 5 E, lanes 1 and 2). Similarly, F-actin and MTs both remained in the su-

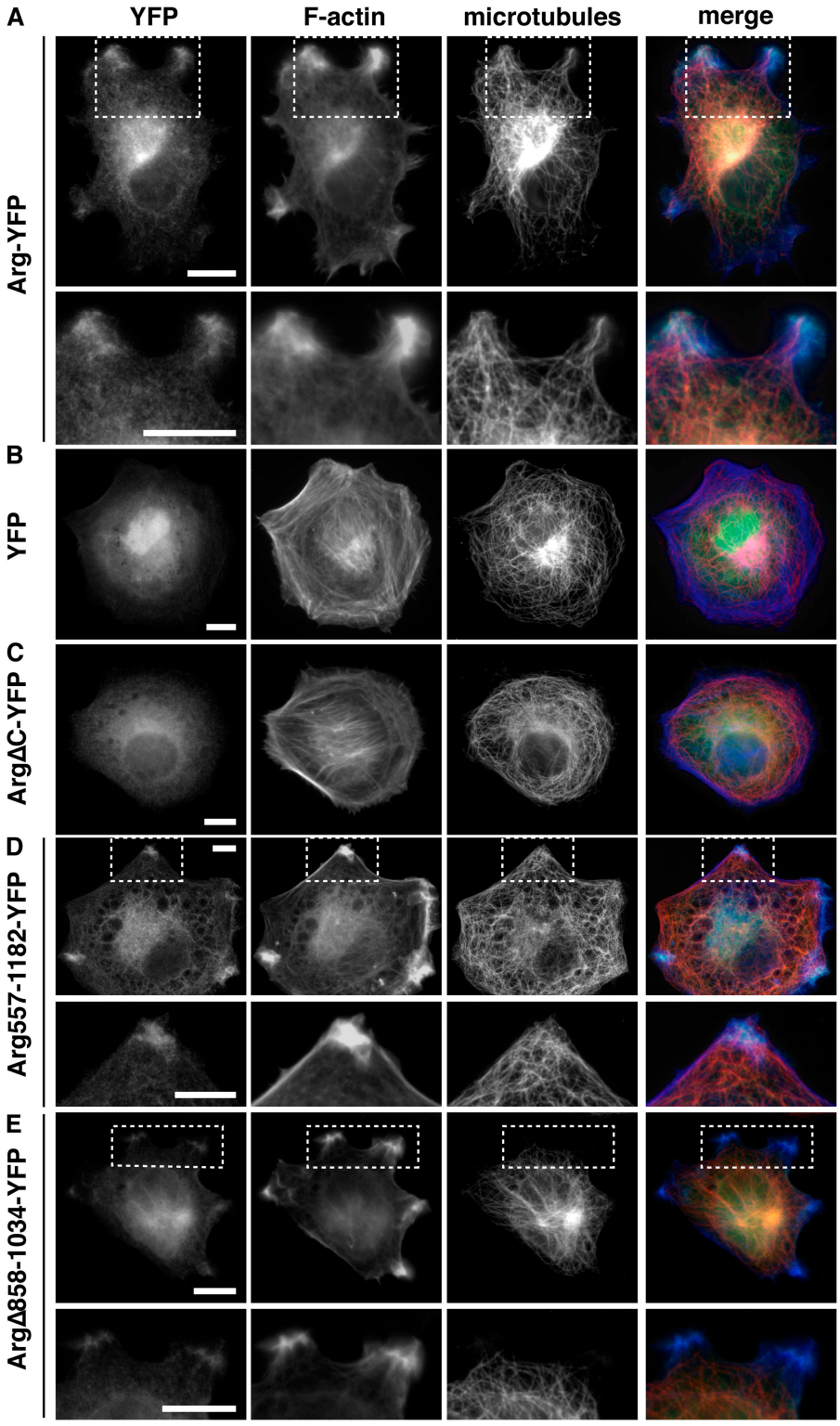

Figure 6. **Arg-YFP mediates interactions between F-actin and MTs at the cell periphery.** (A–E) *arg*$^{-/-}$ fibroblasts expressing Arg-YFP or Arg mutant-YFP fusions (green) were stained with anti-tubulin antibodies followed by Alexa 594–labeled secondary antibodies to visualize MTs (red) and with Alexa 350-phalloidin to visualize F-actin (blue). (A) *arg*$^{-/-}$ cells expressing Arg-YFP; panels in the second row are enlargements of the boxed regions in the first row, showing that the MT-rich protrusions induced in Arg-YFP–expressing cells colocalize with Arg-YFP concentrations and F-actin–rich structures. (B–E) *arg*$^{-/-}$ cells expressing YFP (B), ArgΔC-YFP (C), Arg557-1182-YFP (D), or ArgΔ858-1034-YFP (E). (D and E) Panels in the bottom row are enlargements of the boxed regions in the top row. Bars, 10 μm.

pernatant when the two proteins were mixed (Fig. 5 E, lanes 5 and 6). However, when Arg and F-actin were mixed, Arg bundled F-actin, and some of these bundles were recovered in the low speed pellet (Fig. 5 E, lanes 3 and 4). When Arg, F-actin, and MTs were all mixed, a portion of the MTs cosedimented with the Arg-F-actin bundles (Fig. 5 E, lanes 7 and 8). To rule out the possibility that Arg-F-actin bundles were nonspecifically trapping MTs and forcing them into the pellet, we also tested an Arg mutant (ArgΔ858-1034) that lacked part of the MT-binding domain but retained both F-actin–binding domains. Although it could still bundle F-actin (Fig. 5 F, lanes 3 and 4), ArgΔ858-1034 had a greatly reduced ability to recruit MTs into F-actin bundles (Fig. 5 F, lanes 7 and 8). Together, these results demonstrate that Arg can use its F-actin–binding domains and MT-binding domain to cross-link MTs and F-actin bundles in vitro.

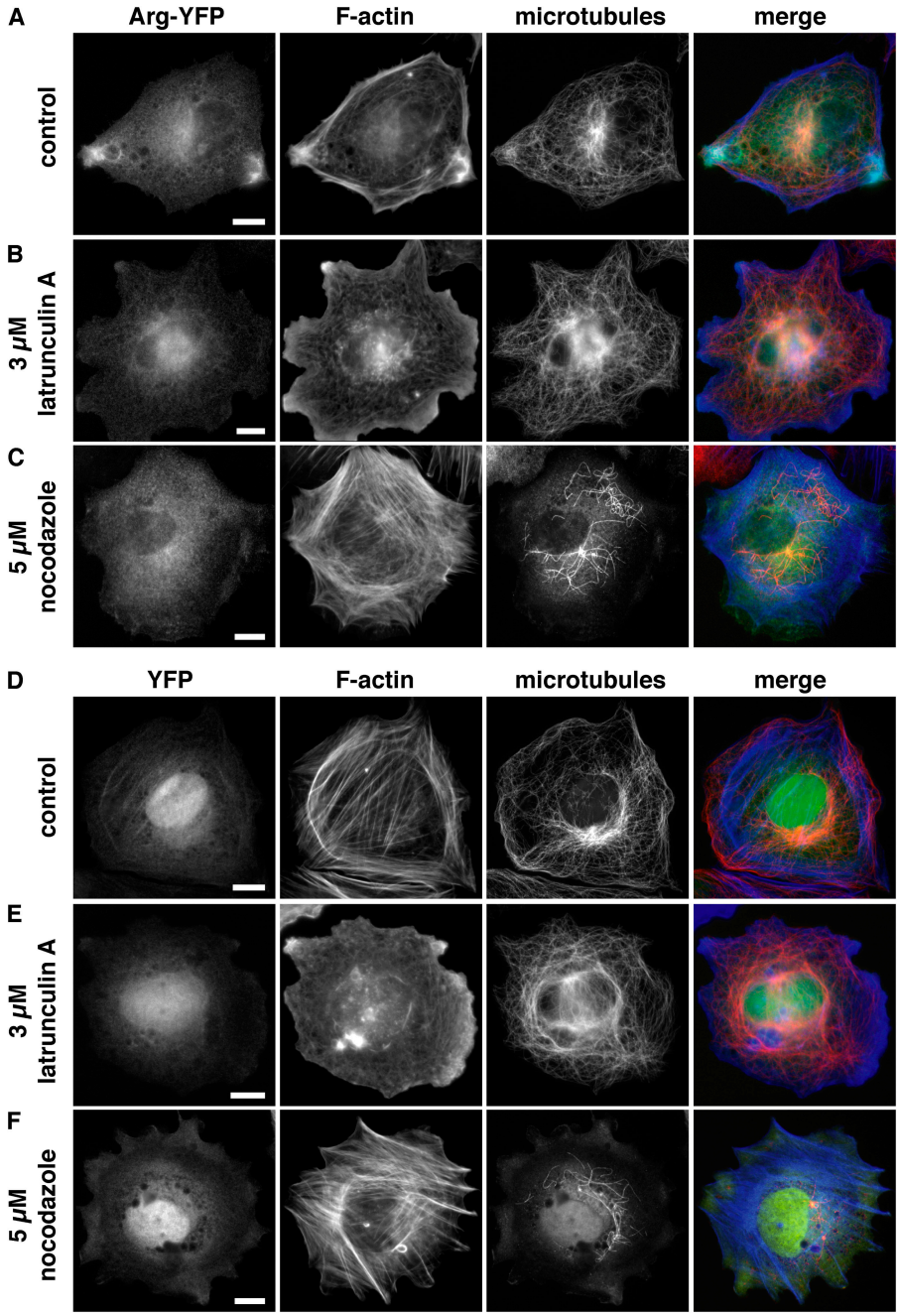

Figure 7. **Arg concentration at the cell periphery requires intact F-actin and MTs.** *arg*$^{-/-}$ fibroblasts expressing Arg-YFP (A–C; green) or YFP (D–F; green) were plated on fibronectin-coated coverslips and were treated with DMSO (drug vector control), latrunculin A, or nocodazole for 30 min. The cells were then fixed and stained for MTs (red) and F-actin (blue). Arg-YFP–expressing cells treated with (A) DMSO. Treatment with (B) 3 μM latrunculin A or (C) 5 μM nocodazole disrupted the Arg-YFP concentrations at the cell periphery. YFP-expressing cells treated with (D) DMSO, (E) 3 μM latrunculin A, or (F) 5 μM nocodazole. Bars, 10 μm.

Arg mediates interactions between F-actin and MTs at the cell periphery

We used fluorescence microscopy to examine whether Arg could use its MT-binding activity to influence MT localization in fibroblasts. Our attempts to localize endogenous Arg in wild-type cells with the currently available antibodies were unsuccessful. It was for this reason we developed a vector to express Arg-YFP at near physiological levels. The ability of Arg-YFP to complement the lamellipodial defects of *arg*$^{-/-}$ cells (Fig. 1, D and F) suggests that the Arg-YFP fusion protein behaves like wild-type Arg. Arg-YFP concentrates in protrusive structures at the cell periphery (Fig. 2, B and C; Fig. 6 A). As we have shown previously, these Arg-YFP concentrations colocalize with F-actin–rich structures (Wang et al., 2001; Fig. 6 A). Regions of intense MT staining were found in association with these Arg-YFP–F-actin concentrations at the cell periphery (Fig. 6 A). The Arg-YFP localization and enriched MT staining did not coincide completely. Instead, individual MTs appeared to join together, extending from the center of the cell toward discrete sites of Arg-YFP–F-actin concentrations at the cell periphery. Peripheral F-actin–MT concentrations were not observed in control YFP-expressing fibroblasts (Fig. 6 B), where the YFP signal was distributed diffusely throughout the nucleus and cytoplasm.

Because Arg appears to tether actin and MTs together at the periphery of the cell, we tested whether the association of Arg-YFP with F-actin–MT-rich concentrations was sensitive to the disruption of F-actin or MTs by treating *arg*$^{-/-}$ fibroblasts expressing Arg-YFP (Fig. 7, A–C) or YFP (Fig. 7, D–F) with latrunculin A or nocodazole, respectively. In control

YFP-expressing cells treated with 3 μM latrunculin A, the actin filaments were completely depolymerized (compare Fig. 7 E with Fig. 7 D); however, some F-actin signal remained in the exaggerated lamellipodia caused by latrunculin A (Fig. 7 E). When Arg-YFP–expressing *arg*$^{-/-}$ fibroblasts were treated with 3 μM latrunculin A, the Arg-YFP concentrations at the periphery of the cell were disrupted (compare Fig. 7 B with Fig. 7 A). In control YFP-expressing *arg*$^{-/-}$ fibroblasts, treatment with 5 μM nocodazole disrupted almost all MTs, leaving a few MTs localized around the centrosome (compare Fig. 7 F with Fig. 7 D). Treatment of Arg-YFP–expressing cells with 5 μM nocodazole disrupted the Arg-YFP concentrations at the cell periphery (compare Fig. 7 C with Fig. 7 A). These observations suggest that the Arg-YFP concentrations at protrusive structures in the cell periphery require intact F-actin and MTs.

The Arg COOH-terminal half requires the MT-binding domain to promote formation of F-actin–MT-rich structures

We examined fibroblasts expressing YFP-tagged Arg deletion mutants to determine which domains of Arg were required to promote formation of F-actin–MT-rich structures at the cell periphery. ArgΔC-YFP, an Arg COOH-terminal mutant lacking the F-actin–binding and MT-binding domains, failed to localize to the periphery or promote F-actin–MT concentrations (Fig. 6 C). When expressed on their own, neither the F-actin–binding domains (Arg688-930-YFP, Arg1034-1182-YFP) nor the MT-binding domain (Arg930-1140-YFP) localized to the periphery or affected the cellular F-actin or MT structure (unpublished data). However, Arg557-1182-YFP could direct the formation of the F-actin–MT-rich domains at the periphery (Fig. 6 D). We conclude that the Arg COOH-terminal half (Arg557-1182), which contains both F-actin–binding domains and the MT-binding domain, is necessary and sufficient for the formation of F-actin–MT-rich concentrations at the cell periphery.

We examined the localization of ArgΔ858-1034-YFP, which has reduced MT-binding activity in vitro (Fig. 5 F) to determine whether the Arg MT-binding domain was required for MT targeting to Arg–F-actin clusters. Importantly, ArgΔ858-1034-YFP retains the F-actin–binding domains, both of which are required for clustering of Arg at the cell periphery (Wang et al., 2001). ArgΔ858-1034-YFP was found in discrete clusters with F-actin at the fibroblast periphery (Fig. 6 E). However, MTs target the ArgΔ858-1034-YFP–F-actin clusters with a greatly reduced frequency relative to Arg-YFP–F-actin clusters (compare Fig. 6 E with Fig. 6 A).

The Arg COOH-terminal half requires the MT-binding domain to rescue defects in lamellipodial dynamics of *arg*$^{-/-}$ cells

Because the Arg COOH-terminal half was able to promote F-actin–MT clusters (Fig. 6 D), we tested whether it could rescue the deficient lamellipodial dynamics and membrane ruffling observed in *arg*$^{-/-}$ fibroblasts. Like Arg-YFP–expressing cells, the periphery of Arg557-1182-YFP–expressing *arg*$^{-/-}$ fibroblasts was irregular, containing numerous protrusions (Fig. 8 A; Video 4, available at http://www.jcb.org/cgi/content/full/jcb.200308055/DC1). Kymographs of these cells had the "rolling hill" profile found in wild-type or Arg-YFP–expressing *arg*$^{-/-}$ fibroblasts (Fig. 8 A). The frequencies of lamellipodial protrusion and lamellipodial retraction in the Arg557-1182-YFP–expressing *arg*$^{-/-}$ fibroblasts were restored to levels observed in wild-type cells (Fig. 8 C). Expression of Arg557-1182-YFP in *arg*$^{-/-}$ fibroblasts also led to increased membrane ruffling, although it did not restore the frequency of ruffling to that observed in wild-type cells. Like Arg-YFP, the Arg557-1182-YFP signal was concentrated at protrusions and ruffles (Fig. 6 D). These observations indicate that the activities required for Arg to promote lamellipodial dynamics and membrane protrusions reside in the Arg COOH-terminal half.

To test whether MT-targeting to Arg–F-actin concentrations was important for lamellipodial dynamics, we measured the ability of ArgΔ858-1034-YFP to complement the deficiencies in lamellipodial dynamics in *arg*$^{-/-}$ fibroblasts. Although it could form concentrations with F-actin at the periphery (Fig. 6 E), ArgΔ858-1034 did not rescue the defects in lamellipodial dynamics of *arg*$^{-/-}$ fibroblasts (Fig. 8, B and C; Video 5, available at http://www.jcb.org/cgi/content/full/jcb.200308055/DC1). Interestingly, although the periphery of ArgΔ858-1034-YFP–expressing *arg*$^{-/-}$ cells appeared irregular, with phase-dense protrusions, kymographic analysis revealed that these lamellae were not dynamic, but instead exhibited the more static "prairie-like" kymographs reminiscent of *arg*$^{-/-}$ cells (Fig. 8 B). As a consequence, the shape of ArgΔ858-1034-YFP–expressing cells did not change appreciably during the filming period (Fig. 8 B, compare left two panels), in contrast to Arg-YFP or Arg557-1182-YFP–expressing cells where noticeable shape changes occurred during the filming period (Fig. 8 A, compare left two panels). Despite its inability to restore lamellipodial dynamics, ArgΔ858-1034-YFP did restore the level of phase-dense membrane ruffles in these cells (Fig. 8 C). Our data suggest that the targeting of MTs to peripheral Arg–F-actin clusters is required for Arg to promote lamellipodial protrusion and retraction.

Discussion

We report here that Arg nonreceptor tyrosine kinase modulates lamellipodial dynamics and membrane ruffling in fibroblasts adhering to fibronectin. We show that Arg can use its MT-binding domain and two F-actin–binding domains to mediate interactions between MTs and F-actin in vitro and at sites of lamellipodial protrusion and membrane ruffling in vivo. Deletion of the MT-binding domain disrupts the targeting of MTs to Arg–F-actin clusters and destroys the ability of Arg to promote membrane protrusion. We also demonstrate that the Arg COOH-terminal half is necessary and sufficient to cross-link F-actin and MTs in vitro and to modulate normal lamellipodial behavior in cells. Together, these observations strongly suggest that Arg regulates lamellipodial dynamics and ruffling by mediating physical interactions between MTs and F-actin at the cell periphery.

The Arg COOH-terminal half organizes cytoskeletal structure

Abl family kinases regulate cell motility and neuronal morphogenesis by controlling the structure and function of the

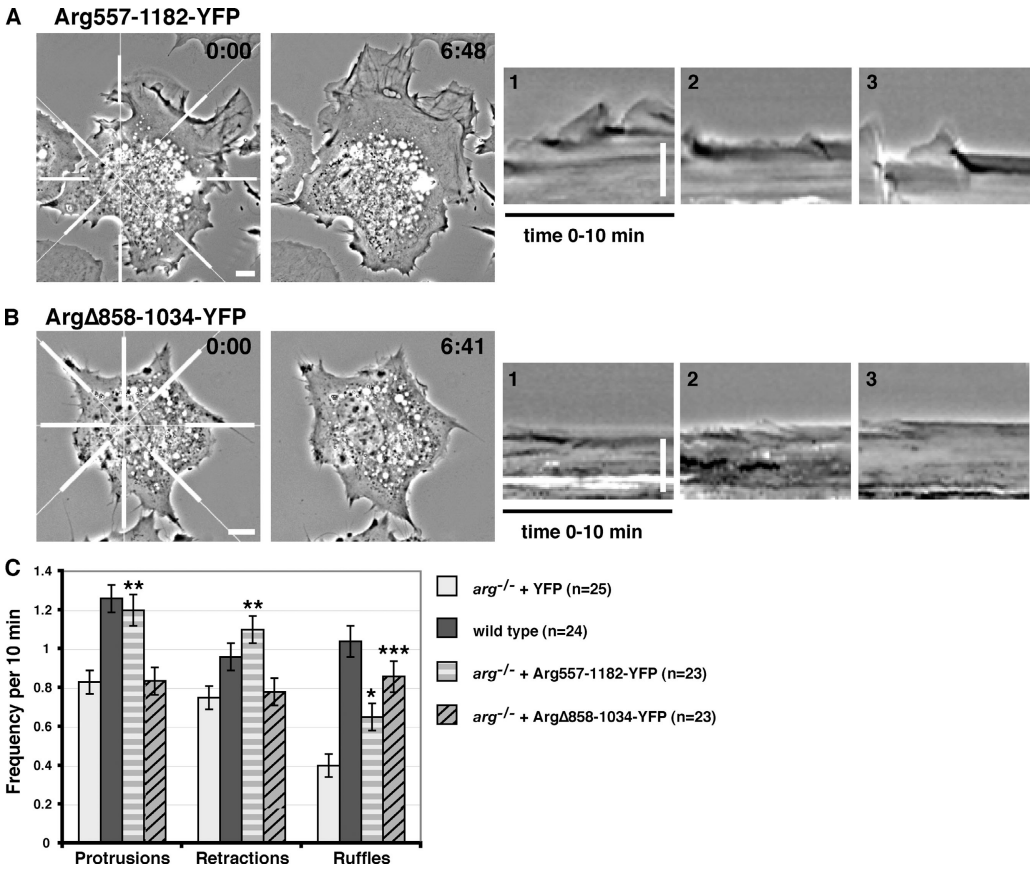

Figure 8. **The Arg COOH-terminal half requires its MT-binding domain to rescue defects in lamellipodial dynamics in *arg*$^{-/-}$ cells.** (A and B) The left two panels in A and B are individual frames from 10-min time-lapse movies of *arg*$^{-/-}$ fibroblasts expressing Arg557-1182-YFP, which contains the F-actin–binding domains and the MT-binding domain (A; Video 4), or ArgΔ858-1034-YFP, which contains both F-actin–binding domains but not the MT-binding domain (B; Video 5). Time elapsed min:s. Examples of kymographs at three of the eight positions around the cell periphery (indicated by thick white bars) for the cells in A and B are shown in the right three panels for each. Time is in the horizontal direction, and distance is in the vertical direction. Bars, 10 μm. (C) Frequencies of membrane protrusion, membrane retraction, and phase-dense membrane ruffles were quantified for *arg*$^{-/-}$ + YFP ($n = 25$), wild-type ($n = 24$), *arg*$^{-/-}$ + Arg557-1182-YFP ($n = 23$), and *arg*$^{-/-}$ + ArgΔ858-1034-YFP ($n = 23$) cells at eight places around the cell periphery for each cell. The differences in frequencies of protrusion, retraction, and ruffling between the *arg*$^{-/-}$ + YFP and *arg*$^{-/-}$ + Arg557-1182-YFP or *arg*$^{-/-}$ + ArgΔ858-1034-YFP cells were statistically significant by *t* test as indicated (*, $P < 0.005$; **, $P < 0.0005$; and ***, $P < 0.00005$). Error bars represent mean ± SEM.

actin cytoskeleton. Our earlier work has shown that Arg can use its two F-actin–binding domains to bundle F-actin in vitro and in vivo and promote F-actin–rich protrusive structures at the cell periphery (Wang et al., 2001). We confirm and extend these findings here by showing that Arg can also bind MTs in vitro and can recruit MTs into the peripheral F-actin–rich structures in cells. We demonstrate that Arg and Arg fragments that retain the ability to cross-link F-actin and MTs in vitro can form these F-actin–MT-rich concentrations at the cell periphery. As part of their function, Abl family kinases relay signals from growth factor (Plattner et al., 1999, 2003) and adhesion receptors (Lewis et al., 1996; Lewis and Schwartz, 1998) to the cytoskeleton. Our results suggest that the Arg COOH-terminal half may link cell surface receptor signaling to discrete sites of interaction between the MT and F-actin cytoskeletons.

We show that upon adhesion to fibronectin, *arg*$^{-/-}$ fibroblasts exhibit fewer episodes of lamellipodial protrusion, lamellipodial retraction, and phase-dense membrane ruffling as compared with wild-type fibroblasts. Expression of Arg-YFP in *arg*$^{-/-}$ fibroblasts rescues these defects. Preliminary observations suggest that Arg-YFP–expressing *arg*$^{-/-}$ cells contain fewer focal adhesions than *arg*$^{-/-}$ cells. This observation may help to explain why Arg-induced lamellipodial protrusions often fail to adhere, leading to the increased frequency of lamellipodial retractions in these cells.

Our studies identified a minimal MT-binding domain in the Arg COOH-terminal half (amino acids 924–1090). A 71–amino acid region within this domain (amino acids 984–1054) shares 37% identity with a COOH-terminal region of dynamin, a cytoplasmic GTPase. MTs can bind the dynamin COOH terminus and activate its GTPase activity in vitro (Herskovits et al., 1993), but it is unclear whether MTs affect dynamin function in vivo. Although it is not homologous to other MT-binding proteins, the Arg MT-binding domain is both basic (pI = 9.85) and proline rich (17%; 28 prolines/166 residues). The MT-binding regions of MAP2 and Tau are also basic and proline rich (Lee et al., 1988). Basic residues in the MAP2/Tau MT-binding regions are believed to form electrostatic interactions with the acidic COOH terminus of tubulin (Serrano et al., 1984, 1985; Al-Bassam et al., 2002). The basic residues in the Arg

MT-binding domain may contribute similarly to MT-binding through interactions with the tubulin COOH terminus.

Arg interacts with F-actin and MTs at the cell periphery

Both Arg and the Arg COOH-terminal half concentrate at the cell periphery. These findings suggest that the F-actin–binding and/or MT-binding domains in the Arg COOH-terminal half localize Arg to the cell periphery. Arg requires its F-actin–binding domains to localize at the periphery (Wang et al., 2001). In vitro, Arg binds cooperatively to F-actin, and this cooperativity could act as a self-concentrating mechanism because it would favor the concentration of Arg to sites where other Arg molecules are already bound. Disruption of MTs with nocodazole inhibits the formation of Arg–F-actin clusters at the periphery (Fig. 7 C), but the MT-binding–defective ArgΔ858-1034 mutant still forms F-actin–rich clusters (Fig. 6 E). These findings suggest that MTs are required for the formation of Arg–F-actin clusters, but may not be absolutely required for Arg localization to the periphery.

As they extend to the periphery, MTs make two distinct types of interactions with F-actin. First, MTs extend along "guides" of bundled actin filaments (Rodriguez et al., 2003; Salmon et al., 2002; Schaefer et al., 2002). MTs are tethered to F-actin bundles during this process via side-to-side cross-links, but these cross-linking proteins are not known. Second, the growing ends of MTs are associated with a "tip complex" containing the EB1 and APC proteins (Mimori-Kiyosue and Tsukita, 2001; Barth et al., 2002). Upon reaching the periphery, MT plus ends can be captured through interactions of the tip complex with peripheral clusters of F-actin (Mimori-Kiyosue and Tsukita, 2001; Barth et al., 2002). We hypothesize that Arg might be a component of the peripheral target for MT plus ends. We show here that Arg is concentrated into patches at the cell periphery that coincide with regions of increased targeting by MTs. Our experiments show that Arg binding to MTs in vitro saturates at a ratio of 0.82 Arg/1 MT dimer, which is higher than would be expected if Arg bound exclusively to MT plus ends. Arg may bind to the sides of MTs that extend to the periphery. Alternatively, other cellular proteins may restrict Arg binding to the MT plus end in vivo.

Based on our demonstrations that Arg can bundle F-actin (Wang et al., 2001) and can cross-link F-actin and MTs, we predict that the cytoskeletal ultrastructure in Arg-induced protrusive structures will contain cortical F-actin bundles cross-linked to MT sides or MT plus ends. We do not know whether the increased concentration of MTs with Arg and F-actin at the cell periphery results from increased MT polymerization or increased stabilization of MTs. This issue may be best addressed by monitoring MTs in Arg-expressing cells using fluorescent speckle microscopy (Waterman-Storer and Salmon, 1999).

Does Arg mediate functional interactions between MTs and Rho family GTPases?

MT extension into the cell periphery is required for the formation of protrusive structures in polarized motile cells (Vasiliev, 1991; Waterman-Storer et al., 1999). Growing evidence indicates that MTs regulate cell polarization by locally regulating the activity of Rho family GTPases (Wittmann and Waterman-Storer, 2001). MT polymerization can activate Rac1 (Waterman-Storer et al., 1999), which could promote membrane protrusion by increasing actin polymerization at the leading edge. Several observations suggest that Abl family kinases may also participate in the regulation of Rac1 activity. Both Rac1 (Nobes et al., 1995) and Abl kinase activities (Plattner et al., 1999) are increased in fibroblasts after treatment with PDGF, and both activities are required for PDGF-induced membrane ruffling (Ridley et al., 1992; Plattner et al., 1999). Rac1 activity is also required for the oncogenic v-Abl protein to promote activation of mitogenically regulated gene expression (Renshaw et al., 1996). Additionally, Rac and Cdc42 are activated after cellular invasion by the bacterial pathogen *Shigella flexneri* (Burton et al., 2003), but Rac and Cdc42 are not activated by *Shigella* in $abl^{-/-}arg^{-/-}$ cells (Burton et al., 2003). Together, with the results presented here, these observations suggest that Abl family kinases might link MT exploration of the periphery to localized Rac1 activation.

MT exploration of the cell periphery is also associated with decreased levels of RhoA activity. MTs inhibit RhoA in part by sequestering GEF1, a Rho activator (Krendel et al., 2002). We have recently found that Arg can also inhibit RhoA by phosphorylating and activating the 190-kD Rho GTPase activating protein (p190RhoGAP), which inhibits RhoA (Hernández et al., 2004b). MTs may also inhibit RhoA by localizing Arg to discrete regions at the cell periphery. Tethered at the cell periphery by its F-actin– and MT-binding domains, Arg may regulate the formation of protrusive structures through the localized activation of Rac1 and inhibition of RhoA.

Materials and methods

Molecular cloning and purification of recombinant proteins

Murine Arg and Arg mutant cDNAs were cloned into the pFastBac HTa expression vector (QIAGEN). Proteins were expressed and purified as described previously (Wang et al., 2001). GST-fusion protein expression vectors were constructed in pGEX-4T-1 (Amersham Biosciences), and proteins were expressed in *Escherichia coli* and purified on glutathione-linked agarose beads (Sigma-Aldrich). Deletion mutants and protein fragments were constructed using the amino acid numbering for the myristoylated form of murine Arg–ArgΔC including amino acids 1–557; ArgΔ930-1140 lacking amino acids 930–1140; ArgΔ858-1034 deleting 858-1034; Arg557-1182; Arg557-1140; Arg930-1140; GST-557-930; GST-930-1140; GST-924-1090; GST-930-1060; GST-930-980; GST-980-1060; GST-1034-1182. YFP-tagged versions of Arg or Arg mutants were constructed using pEYFP-N1 (CLONTECH Laboratories, Inc.), and the YFP fusions were subcloned into the PX1 retroviral vector.

Cell culture and retroviral infection

Wild-type or $arg^{-/-}$ fibroblasts were isolated from 13-d-old mouse embryos and spontaneously immortalized by continual passage at 7.5×10^5 cells/10-cm dish for 15–20 passages. Retroviruses expressing Arg or Arg mutants fused to YFP were prepared according to standard techniques (Pear et al., 1993). After infection of $arg^{-/-}$ cells with these retroviruses, immunoblotting with anti-YFP antibodies (CLONTECH Laboratories, Inc.) revealed that each YFP-fusion protein was of the expected size and was expressed at similar levels in infected cells. For semiquantitative Western blotting, cell lysates from wild-type cells and $arg^{-/-}$ cells infected with Arg-YFP and sorted for YFP signal were prepared, and the protein concentration was determined using a BCA kit (Pierce Chemical Co.). A dilution series of cell lysate and of purified Arg protein was separated by SDS-PAGE, immunoblotted with α-Arg antibodies, and quantitated using a Mo-

lecular Dynamics Densitometer. Arg-YFP was expressed at a 2.3-fold greater level than the endogenous Arg level, and Arg557-1182-YFP and ArgΔ858-1034-YFP were expressed at similar levels to Arg-YFP.

Immunofluorescence microscopy

Cells were plated on glass coverslips coated with 10 μg/ml fibronectin (Sigma-Aldrich) and blocked with 1% BSA (GIBCO BRL) 48–72 h after infection and were allowed to attach for 30 min. Cells were rinsed before fixation with PHEM buffer (60 mM Pipes, 25 mM Hepes, 10 mM EDTA, 2 mM $MgCl_2$, pH 6.9) that was prewarmed to 37°C. Cells were fixed with 4% PFA (prewarmed to 37°C) for 20 min at RT and then permeabilized with 0.5% or 1% Triton X-100 for 10 min. Cells were stained with anti–α-tubulin antibodies (clone DM 1A; Sigma-Aldrich), Alexa 594–labeled secondary antibodies (Molecular Probes), and Alexa 350-phalloidin (Molecular Probes). Cells were imaged on a microscope (model TE2000-S; Nikon) at 40× or 100×.

Stock solutions of nocodazole (Sigma-Aldrich) or latrunculin A (Sigma-Aldrich) were dissolved in DMSO. Nocodazole or latrunculin A was diluted in growth media at the concentrations indicated in the figure legends and added to cells for 30 min at 37°C before fixation. Control cells were treated with DMSO alone.

Time-lapse microscopy and kymography

For time-lapse microscopy, cells were adapted to microscopy media (growth media with 10 mM Hepes [GIBCO BRL]) for ∼16 h and plated on fibronectin-coated, BSA-blocked glass coverslips. Cells were imaged between 30 min and 2 h after plating using a microscope (model TE2000-S; Nikon) driven by Openlab software (Improvision). Cells were maintained at 37°C during imaging with an in-line flow heater and a heated chamber (Warner Instruments). 40× phase contrast and YFP movies were ∼10 min long with frames taken every ∼10–12 s as noted in figure legends.

For kymography, phase-contrast time-lapse sequences were obtained as described above. Each cell was overlaid with a template containing eight equally spaced radiating lines with the center located on the cell nucleus. Kymographs were made along each of the eight lines at the intersecting point along the cell periphery using ImageJ software (NIH). Kymographs were analyzed for frequency of lamellipodial protrusions, retractions, and phase-dense ruffles as described by Hinz and colleagues (Hinz et al., 1999).

Cosedimentation assays

Phosphocellulose-purified tubulin was prepared from frozen chick brains following the protocol described in Hyman et al. (1991). Tubulin was polymerized at a final concentration of 18 μM at 37°C for 30 min. The polymerization buffer contained 100 mM Pipes, pH 6.8, 1 mM $MgSO_4$, 1 mM EGTA, 1 mM GTP, and 15 nM paclitaxel. For binding assays, 0.25 μM Arg or Arg mutant protein was mixed with increasing concentrations of MTs (0–8 μM) at 25°C for 15 min in a binding buffer containing 20 mM Pipes, pH 6.8, 100 mM KCL, 1 mM DTT, 1 mM GTP, and 15 nM paclitaxel. Mixtures were pelleted by centrifugation at 120,000 *g* for 30 min at 20°C. As a control, Arg or Arg mutant protein was subjected to centrifugation alone, in the absence of MTs. The pellet (P) and supernatant (S) fractions were recovered and separated by SDS-PAGE and stained with Coomassie blue. Protein bands were quantified by densitometry. GST-924-1090 had similar mobility to tubulin on a SDS-PAGE gel. Therefore, the amount of GST-924-1090 in the pellet and supernatant fractions was determined by immunoblotting with α-GST antibodies (Santa Cruz Biotechnology, Inc.). Binding affinity was determined from the concentration of Arg bound to MTs for each concentration of MTs in the assays as per Blanchoin and Pollard (1998). Data were analyzed using KaleidaGraph software (Synergy Software) and fitted to Eq. 1, where $r = [Arg]_{total}$, $x = [MT]_{total}$, $y = [Arg]_{bound}$, and K_d is the dissociation constant of the Arg–MT complex.

$$y = \frac{(r + K_d + x) - \sqrt{(r + K_d + x)^2 - 4(rx)}}{2}. \quad (1)$$

Fluorescence assay for F-actin–MT cross-linking

Rhodamine-labeled MTs were stabilized by paclitaxel, and F-actin was stabilized by a 1:4 mix of phalloidin/Alexa 488-phalloidin. Purified Arg or Arg mutant proteins (0.5 μM) were mixed with 1 μM MTs at 25°C for 10 min. After F-actin addition (1 μM), the mixture was incubated for an additional 15 min. The mixture was then diluted fivefold (or twofold for Arg557-930) and visualized by fluorescence microscopy at 63× magnification.

Cosedimentation assay for F-actin–MT cross-linking

MTs were polymerized as described above. F-actin was prepared as described previously (Wang et al., 2001). 1 μM Arg or 1 μM ArgΔ858-1034 was incubated with 1 μM MTs in binding buffer at 25°C for 10 min. After addition of 1 μM F-actin, the reaction was incubated for an additional 15 min at 25°C. The mixture was pelleted by centrifugation at 5,000 *g* for 10 min at 20°C to pellet F-actin bundles and associated proteins. The pellet (P) and supernatant (S) fractions were recovered, separated by SDS-PAGE, and visualized using Coomassie blue staining. Controls included the incubation and centrifugation of Arg or ArgΔ858-1034 alone, Arg or ArgΔ858-1034 with MTs or F-actin, and MTs with F-actin.

Online supplemental material

Video 1 shows phase-contrast and fluorescence time-lapse movies of an $arg^{-/-}$ fibroblast expressing YFP (Fig. 2 A). Video 2 shows phase-contrast and fluorescence time-lapse movies of an $arg^{-/-}$ fibroblast expressing Arg-YFP (Fig. 2 B). Video 3 shows time-lapse movies of an enlargement of one of the protrusive structures induced by Arg-YFP (Fig. 2 C). Video 4 shows a phase-contrast time-lapse movie of an $arg^{-/-}$ fibroblast expressing Arg557-1182-YFP (Fig. 8 A). Video 5 shows a phase-contrast time-lapse movie of an $arg^{-/-}$ fibroblast expressing ArgΔ858-1034-YFP (Fig. 8 B). Fig. S1 shows that Arg-YFP concentration at the cell periphery is not due to increased cell volume. Fig. S2 shows the saturation stoichiometry of Arg/MT binding. Fig. S3 shows the sequence alignment of the Arg MT-binding domain with residues in the COOH-terminal of dynamin that have been reported to bind MTs. Online supplemental material is available at http://www.jcb.org/cgi/content/full/jcb.200308055/DC1.

We are grateful to Xianyun Ye for technical assistance; members of the Koleske lab, Shelley Halpain, Thomas Pollard, Peter Takizawa, Julie Theriot, and David Van Vactor for helpful discussions and comments on the manuscript; Lee Ligon, Erika Holzbaur, Jim Bear, and Derek Toomre for experimental advice; and John E. Miller for his work on the prairie.

A.L. Miller is supported by predoctoral National Research Service Award (NS045477). A.J. Koleske is a National Alliance for Research on Schizophrenia and Depression Young Investigator and a Scholar of the Leukemia and Lymphoma Society of America. This work was supported by U.S. Public Health Service Research grants DK55389 and DK25387 (to M.S. Mooseker) and NS39475 (to A.J. Koleske).

Submitted: 11 August 2003
Accepted: 10 March 2004

References

Al-Bassam, J., R.S. Ozer, D. Safer, S. Halpain, and R.A. Milligan. 2002. MAP2 and tau bind longitudinally along the outer ridges of microtubule protofilaments. *J. Cell Biol.* 157:1187–1196.

Barth, A.I., K.A. Siemers, and W.J. Nelson. 2002. Dissecting interactions between EB1, microtubules and APC in cortical clusters at the plasma membrane. *J. Cell Sci.* 115:1583–1590.

Bashaw, G.J., T. Kidd, D. Murray, T. Pawson, and C.S. Goodman. 2000. Repulsive axon guidance: Abelson and Enabled play opposing roles downstream of the roundabout receptor. *Cell.* 101:703–715.

Bershadsky, A.D., E.A. Vaisberg, and J.M. Vasiliev. 1991. Pseudopodial activity at the active edge of migrating fibroblast is decreased after drug-induced microtubule depolymerization. *Cell Motil. Cytoskeleton.* 19:152–158.

Blanchoin, L., and T.D. Pollard. 1998. Interaction of actin monomers with Acanthamoeba actophorin (ADF/cofilin) and profilin. *J. Biol. Chem.* 273: 25106–25111.

Burton, E.A., R. Plattner, and A.M. Pendergast. 2003. Abl tyrosine kinases are required for infection by Shigella flexneri. *EMBO J.* 22:5471–5479.

Etienne-Manneville, S., and A. Hall. 2001. Integrin-mediated activation of Cdc42 controls cell polarity in migrating astrocytes through PKCzeta. *Cell.* 106: 489–498.

Etienne-Manneville, S., and A. Hall. 2003a. Cdc42 regulates GSK-3beta and adenomatous polyposis coli to control cell polarity. *Nature.* 421:753–756.

Etienne-Manneville, S., and A. Hall. 2003b. Cell polarity: Par6, aPKC and cytoskeletal crosstalk. *Curr. Opin. Cell Biol.* 15:67–72.

Frasca, F., P. Vigneri, V. Vella, R. Vigneri, and J.Y. Wang. 2001. Tyrosine kinase inhibitor STI571 enhances thyroid cancer cell motile response to hepatocyte growth factor. *Oncogene.* 20:3845–3856.

Gertler, F.B., R.L. Bennett, M.J. Clark, and F.M. Hoffmann. 1989. *Drosophila* abl tyrosine kinase in embryonic CNS axons: a role in axonogenesis is revealed through dosage-sensitive interactions with disabled. *Cell.* 58:103–113.

Giniger, E. 1998. A role for Abl in Notch signaling. *Neuron.* 20:667–681.

Grevengoed, E.E., J.J. Loureiro, T.L. Jesse, and M. Peifer. 2001. Abelson kinase regulates epithelial morphogenesis in *Drosophila*. *J. Cell Biol.* 155:1185–1198.

Gundersen, G.G. 2002. Evolutionary conservation of microtubule-capture mechanisms. *Nat. Rev. Mol. Cell Biol.* 3:296–304.

Hernández, S.E., M. Krishnaswami, A.L. Miller, and A.J. Koleske. 2004a. How do Abl family kinases regulate cell shape and movement? *Trends Cell Biol.* 14: 36–44.

Hernández, S.E., J. Settleman, and A.J. Koleske. 2004b. Adhesion-dependent regulation of p190RhoGAP in the developing brain by the Abl-related gene tyrosine kinase. *Curr. Biol.* 14:691–696.

Herskovits, J.S., H.S. Shpetner, C.C. Burgess, and R.B. Vallee. 1993. Microtubules and Src homology 3 domains stimulate the dynamin GTPase via its C-terminal domain. *Proc. Natl. Acad. Sci. USA.* 90:11468–11472.

Hinz, B., W. Alt, C. Johnen, V. Herzog, and H.W. Kaiser. 1999. Quantifying lamella dynamics of cultured cells by SACED, a new computer-assisted motion analysis. *Exp. Cell Res.* 251:234–243.

Howe, A.K., B.P. Hogan, and R.L. Juliano. 2002. Regulation of vasodilator-stimulated phosphoprotein phosphorylation and interaction with Abl by protein kinase A and cell adhesion. *J. Biol. Chem.* 277:38121–38126.

Hyman, A., D. Drechsel, D. Kellogg, S. Salser, K. Sawin, P. Steffen, L. Wordeman, and T. Mitchison. 1991. Preparation of modified tubulins. *Methods Enzymol.* 196:478–485.

Kain, K.H., and R.L. Klemke. 2001. Inhibition of cell migration by Abl family tyrosine kinases through uncoupling of Crk-CAS complexes. *J. Biol. Chem.* 276:16185–16192.

Kirschner, M., and T. Mitchison. 1986. Beyond self-assembly: from microtubules to morphogenesis. *Cell.* 45:329–342.

Koleske, A.J., A.M. Gifford, M.L. Scott, M. Nee, R.T. Bronson, K.A. Miczek, and D. Baltimore. 1998. Essential roles for the Abl and Arg tyrosine kinases in neurulation. *Neuron.* 21:1259–1272.

Krendel, M., F.T. Zenke, and G.M. Bokoch. 2002. Nucleotide exchange factor GEF-H1 mediates cross-talk between microtubules and the actin cytoskeleton. *Nat. Cell Biol.* 4:294–301.

Lee, G., N. Cowan, and M. Kirschner. 1988. The primary structure and heterogeneity of tau protein from mouse brain. *Science.* 239:285–288.

Lewis, J.M., and M.A. Schwartz. 1998. Integrins regulate the association and phosphorylation of paxillin by c-Abl. *J. Biol. Chem.* 273:14225–14230.

Lewis, J.M., R. Baskaran, S. Taagepera, M.A. Schwartz, and J.Y. Wang. 1996. Integrin regulation of c-Abl tyrosine kinase activity and cytoplasmic-nuclear transport. *Proc. Natl. Acad. Sci. USA.* 93:15174–15179.

Mimori-Kiyosue, Y., and S. Tsukita. 2001. Where is APC going? *J. Cell Biol.* 154: 1105–1109.

Mitchison, T.J., and L.P. Cramer. 1996. Actin-based cell motility and cell locomotion. *Cell.* 84:371–379.

Moresco, E.M., and A.J. Koleske. 2003. Regulation of neuronal morphogenesis and synaptic function by Abl family kinases. *Curr. Opin. Neurobiol.* 13:535–544.

Nobes, C.D., P. Hawkins, L. Stephens, and A. Hall. 1995. Activation of the small GTP-binding proteins rho and rac by growth factor receptors. *J. Cell Sci.* 108(Pt 1):225–233.

Pear, W.S., G.P. Nolan, M.L. Scott, and D. Baltimore. 1993. Production of high-titer helper-free retroviruses by transient transfection. *Proc. Natl. Acad. Sci. USA.* 90:8392–8396.

Plattner, R., L. Kadlec, K.A. DeMali, A. Kazlauskas, and A.M. Pendergast. 1999. c-Abl is activated by growth factors and Src family kinases and has a role in the cellular response to PDGF. *Genes Dev.* 13:2400–2411.

Plattner, R., B.J. Irvin, S. Guo, K. Blackburn, A. Kazlauskas, R.T. Abraham, J.D. York, and A.M. Pendergast. 2003. A new link between the c-Abl tyrosine kinase and phosphoinositide signalling through PLC-gamma1. *Nat. Cell Biol.* 5:309–319.

Pollard, T.D., and G.G. Borisy. 2003. Cellular motility driven by assembly and disassembly of actin filaments. *Cell.* 112:453–465.

Renshaw, M.W., E. Lea-Chou, and J.Y. Wang. 1996. Rac is required for v-Abl tyrosine kinase to activate mitogenesis. *Curr. Biol.* 6:76–83.

Renshaw, M.W., J.M. Lewis, and M.A. Schwartz. 2000. The c-Abl tyrosine kinase contributes to the transient activation of MAP kinase in cells plated on fibronectin. *Oncogene.* 19:3216–3219.

Ridley, A.J., H.F. Paterson, C.L. Johnston, D. Diekmann, and A. Hall. 1992. The small GTP-binding protein rac regulates growth factor-induced membrane ruffling. *Cell.* 70:401–410.

Rodriguez, O.C., A.W. Schaefer, C.A. Mandato, P. Forscher, W.M. Bement, and C.M. Waterman-Storer. 2003. Conserved microtubule-actin interactions in cell movement and morphogenesis. *Nat. Cell Biol.* 5:599–609.

Rothenberg, M.E., S.L. Rogers, R.D. Vale, L.Y. Jan, and Y.N. Jan. 2003. *Drosophila* pod-1 crosslinks both actin and microtubules and controls the targeting of axons. *Neuron.* 39:779–791.

Salgia, R., B. Brunkhorst, E. Pisick, J.L. Li, S.H. Lo, L.B. Chen, and J.D. Griffin. 1995. Increased tyrosine phosphorylation of focal adhesion proteins in myeloid cell lines expressing p210BCR/ABL. *Oncogene.* 11:1149–1155.

Salmon, W.C., M.C. Adams, and C.M. Waterman-Storer. 2002. Dual-wavelength fluorescent speckle microscopy reveals coupling of microtubule and actin movements in migrating cells. *J. Cell Biol.* 158:31–37.

Schaefer, A.W., N. Kabir, and P. Forscher. 2002. Filopodia and actin arcs guide the assembly and transport of two populations of microtubules with unique dynamic parameters in neuronal growth cones. *J. Cell Biol.* 158:139–152.

Serrano, L., J. Avila, and R.B. Maccioni. 1984. Controlled proteolysis of tubulin by subtilisin: localization of the site for MAP2 interaction. *Biochemistry.* 23: 4675–4681.

Serrano, L., E. Montejo de Garcini, M.A. Hernandez, and J. Avila. 1985. Localization of the tubulin binding site for tau protein. *Eur. J. Biochem.* 153:595–600.

Suter, D.M., and P. Forscher. 1998. An emerging link between cytoskeletal dynamics and cell adhesion molecules in growth cone guidance. *Curr. Opin. Neurobiol.* 8:106–116.

Vasiliev, J.M. 1991. Polarization of pseudopodial activities: cytoskeletal mechanisms. *J. Cell Sci.* 98:1–4.

Wang, Y., A.L. Miller, M.S. Mooseker, and A.J. Koleske. 2001. The Abl-related gene (Arg) nonreceptor tyrosine kinase uses two F-actin-binding domains to bundle F-actin. *Proc. Natl. Acad. Sci. USA.* 98:14865–14870.

Waterman-Storer, C.M., and E.D. Salmon. 1999. Fluorescent speckle microscopy of microtubules: how low can you go? *FASEB J.* 13(Suppl 2):S225–S230.

Waterman-Storer, C.M., R.A. Worthylake, B.P. Liu, K. Burridge, and E.D. Salmon. 1999. Microtubule growth activates Rac1 to promote lamellipodial protrusion in fibroblasts. *Nat. Cell Biol.* 1:45–50.

Wills, Z., J. Bateman, C.A. Korey, A. Comer, and D. Van Vactor. 1999a. The tyrosine kinase Abl and its substrate enabled collaborate with the receptor phosphatase Dlar to control motor axon guidance. *Neuron.* 22:301–312.

Wills, Z., L. Marr, K. Zinn, C.S. Goodman, and D. Van Vactor. 1999b. Profilin and the Abl tyrosine kinase are required for motor axon outgrowth in the *Drosophila* embryo. *Neuron.* 22:291–299.

Wittmann, T., and C.M. Waterman-Storer. 2001. Cell motility: can Rho GTPases and microtubules point the way? *J. Cell Sci.* 114:3795–3803.

Zukerberg, L.R., G.N. Patrick, M. Nikolic, S. Humbert, C.L. Wu, L.M. Lanier, F.B. Gertler, M. Vidal, R.A. Van Etten, and L.H. Tsai. 2000. Cables links Cdk5 and c-Abl and facilitates Cdk5 tyrosine phosphorylation, kinase upregulation, and neurite outgrowth. *Neuron.* 26:633–646.